Lab on a Chip

Dynamic Article Links

Cite this: *Lab Chip*, 2012, **12**, 2309–2312

www.rsc.org/loc

TECHNICAL INNOVATION

Methods to array photonic crystal microcavities for high throughput high sensitivity biosensing on a silicon-chip based platform

Yi Zou,*[a] Swapnajit Chakravarty,*[b] Wei-Cheng Lai,[a] Che-Yun Lin[a] and Ray T. Chen[ab]

Received 19th January 2012, Accepted 13th March 2012
DOI: 10.1039/c2lc40081b

We experimentally demonstrate a method to create large-scale chip-integrated photonic crystal sensor microarrays by combining the optical power splitting characteristics of multi-mode interference (MMI) power splitters and transmission drop resonance characteristics of multiple photonic crystal microcavities arrayed along the length of the same photonic crystal waveguide. L13 photonic crystal microcavities are employed which show high Q values ($\sim$9300) in the bio-ambient phosphate buffered saline (PBS) as well as high sensitivity, experimentally demonstrated to $\sim$98 atto-grams. Two different probe antibodies were specifically detected simultaneously with a control sample, in the same experiment.

1 Introduction

Microarrays provide an unprecedented opportunity for comprehensive concurrent analysis of thousands of biomolecules such as proteins,[1] genes, DNA molecules, small molecules or nucleic acids. The global analysis of the response to a toxic agent, as opposed to the traditional method of examining a few select biomolecules, provides a more complete picture of toxicologically significant events. In proteomics studies for the detection of various infectious diseases and cancers, microarrays have been used ubiquitously. The measurement throughput in such methods is however low due to the necessity to measure each sensor spot separately with an individual detector, which also increases the detection antibody requirement as well as the sample volume needed for measurement.

Label-free biosensors are particularly attractive since they avoid complex chemistries caused by steric hindrance of the labels. All methods of detection transduce the specific binding of the biomolecule of interest to its specific conjugate biomolecule receptor bound to the device substrate, into an electrical, mechanical or optical signal. Optical detection techniques are generally preferred due to their freedom from electromagnetic interference. While several platforms based on ring resonators,[2,3] wire waveguides[4] and surface plasmon resonance (SPR)[5] have been investigated. Photonic crystal (PC) microcavities,[6] in general, are more compact (of the order of a few square microns in surface area) and have higher sensitivity than other devices due to slow light effect and a larger optical mode overlap with the analyte within compact optical mode volume. Recent research has shown that PC biosensors have biomolecular surface mass density detection limit of 22 pg mm^{-2} which compares quite favorably with detection limits of 1 pg mm^{-2} in SPR on almost four orders of magnitude smaller surface area.[7] In contrast to conventional notion of trying to achieve the smallest possible PC microcavity for sensing purposes, we showed that a slightly longer PC microcavity can deliver significantly improved performance both in terms of higher sensitivity as well the ability to detect small changes in concentration. Increasing the length of the PC microcavities reduced the radiation loss, which scales inversely with the cavity length, thereby reducing the resonance linewidth and thus increasing the ability to detect small changes in concentration. Furthermore, the slightly increased length enables larger overlap of the optical mode with the analyte leading to higher sensitivity. The increased length of the PC microcavities is not a drawback in terms of chip scale miniaturization, since a primary requirement in such hybrid architectures is the need to functionalize the resonators with target receptor biomolecules that will bind specifically to their probe biomolecule conjugates in a diagnostic assay. The ink-jet printed target receptor spot size we achieved is about 35 μm in diameter,[7] which thus determines the minimum spacing that can be achieved between adjacent resonators functionalized with different unique target receptor biomolecules in a chip-integrated diagnostic microarray.

In addition, much of the research in the literature concerns single PC microcavity biosensors. Methods to array two-dimensional PC microcavities have primarily focused on the detection of a single biomolecular probe binding to its specific conjugate target biomolecule on all microcavities.[8] In this paper, we demonstrate the high sensitivity of long PC microcavities. We also demonstrate two methods to array these PC microcavities, which can be combined to create large chip-integrated microarrays in which all PC microcavity sensors, each coated with a different biomolecule target receptor, can be simultaneously interrogated with the same small quantity of probe sample, resulting in high throughput diagnostic assays. All devices are

[a]*Department of Electrical and Computer Engineering, University of Texas Austin, TX, 78712. E-mail: raychen@uts.cc.utexas.edu*
[b]*Omega Optics Inc., Austin, TX, 78759. E-mail: swapnajit.chakravarty@omegaoptics.com*

demonstrated in a silicon-on-insulator (SOI) platform, which also guarantees higher fabrication yield, more robust devices, and demonstrates better performance characteristics than the best devices demonstrated to date in the PC platforms on free-standing membranes.

2 Device design

Fig. 1(a) shows the schematic of the test system on chip (SoC), where individual components are clearly shown.

On each output arm of the 1 × 4 multi-mode interference (MMI) studied here, photonic crystal (PC) microcavities are arrayed along the length of a single photonic crystal waveguide (PCW). The test SoC we designed and then fabricated has one PC microcavity on three arms. On the fourth arm, two PC microcavities are arrayed along the length of one PCW. The scanning electron micrograph (SEM) of the key sections is shown in Fig. 2(a) which consists of a 1 × 4MMI optical power splitter which splits the input light from a ridge waveguide into four output channels.

The MMI was simulated by two-dimensional beam propagation method using RSoft's BeamProp software using design rules laid down previously.[9] The simulation result is shown in Fig. 2(b). The length and width of the MMI were designed as 123 μm and 16 μm respectively. Each of the input and output waveguide arms after the 1 × 4MMI is 2.5 μm wide and the output waveguides are separated by 1.5 μm. The output arms of the MMI are numbered as shown in Fig. 2(a). The PCW is a W1 line defect waveguide with uniform lattice constant a = 400 nm, where W1 denotes that width of the PCW is $\sqrt{3}(a)$. Silicon slab thickness and air hole diameter are $h = 0.58a$ and $d = 0.54a$.

Since the ink-jet spot size is 35 μm in diameter, we are pursuing optimized designs investigating sensitivity *versus* increasing size of the PC microcavity. We have shown earlier that L13 PC microcavities with dimensions ~5.5 μm × 0.5 μm, not only have high sensitivity due to overlap of the confined optical mode with more air holes along the periphery of the PC microcavity but also have high quality factor (Q-factors), $Q \approx$ 26 760, which enables the detection of smaller changes in concentration.[7] Linear L13 PC microcavities with 13 missing holes along Γ–K direction, as shown in Fig. 3(a), are fabricated

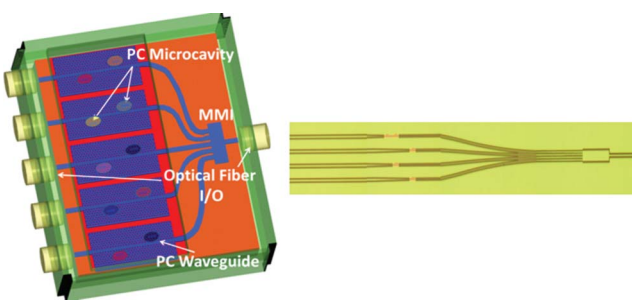

Fig. 1 (a) Generalized schematic of the test system on chip with integrated 1 × xMMI and PC microcavities coupled to PC waveguides. On each of the x output arms of the MMI, multiple PC microcavities are arrayed. Each microcavity is coated with a different target receptor biomolecule, each responsive to its specific conjugate, as indicated by a different color. (b) Stitched microscope image of 1 × 4MMI device studied here.

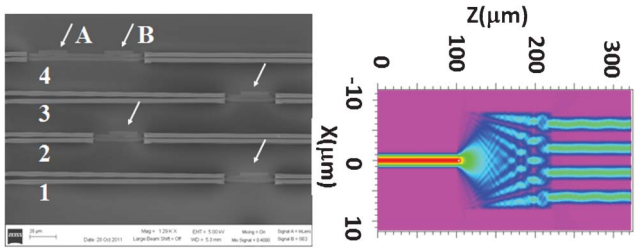

Fig. 2 (a) SEM of PC devices on 4 arms of a 1 × 4MMI (b) Simulation showing optical power distribution in 1 × 4MMI.

two periods away from the PCW. On arms 1–3, the edge air holes on the axis of the PC microcavity are shifted outward[10] in the Γ–K direction by 0.15a. Shifts beyond 0.15a lead to fabrication challenges with adjacent holes. The mode profile of the resonant mode of interest, as described in Ref. 7, is shown in Fig. 3(b).

On arm 4, both PC microcavities are of the specially designed L13 type. In the PC microcavity labeled A, the edge air-holes are shifted in the Γ–K direction inward by 0.05a. In the other PC microcavity labeled B, the edge air-holes are shifted outward in the Γ–K direction by 0.15a. The inward shift of 0.05a causes the resonant mode to interact more with the edge holes along the axis, thus pulling the resonance up in frequency.[10] The design leads to resonant modes from the two series-arrayed microcavities on the same PCW that are separated by wavelength. The spacing of 50 μm between the two microcavities ensures no cross-talk. As said previously, the spacing of 50 μm is not a drawback since we have shown earlier[7] that our Dimatix ink-jet printer achieved a minimum spacing of 50 μm between adjacent printed target antibodies that each covered a circular area with diameter 35 μm.

3 Device fabrication

Devices were fabricated on SOI wafer with 230 nm top silicon layer and 3 μm buried oxide. 45 nm thermal oxide was grown on top of silicon as an etch mask for pattern transfer. PC waveguides, PC impedance tapers to minimize reflection loss, 1 × 4MMI optical splitters and strip waveguides are patterned in one step with e-beam lithography followed by reactive ion etching.

To enable the biosensing function, the on-chip sensing subsystem (OCSS) was functionalized by treating with 10% by volume 3-aminopropyl-triethoxy-silane (3-APTES) in toluene. It was then washed 3 times in toluene to ensure complete removal of unbound 3-APTES, 3 times in methanol to remove toluene

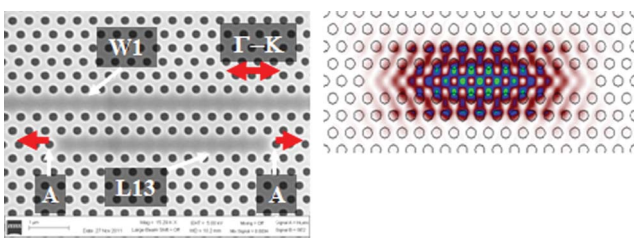

Fig. 3 (a) SEM image of L13 PC microcavity adjacent to a W1 PCW. (b) Electric field intensity profile of the resonance mode of the L13 PC microcavity.

and finally 3 times in de-ionized water to remove methanol. The OCSS was then incubated in 1% glutaraldehyde in phosphate buffered saline (PBS) for 5 min and washed 3 times in PBS and ink-jet printed with target antibodies (Abs) in glycerol. Past research has shown that the 3-APTES-glutaraldehyde coupled layer retains its initial activity for several weeks.[11] This negates any potential concern regarding time-dependent binding affinities of the target Abs, due to the time it takes to switch cartridges in our ink-jet printer. The printed spots were left to incubate overnight. Subsequently, all target Abs not bound to the functionalized device layer were removed by washing 3 times in PBS. The washing steps were completed within a few seconds, which ensures that unbound target Abs do not have sufficient time to bind to undesired areas to create any cross-talk. On arms 1 and 2 of the MMI, as defined in Fig. 2, human IL-10 (Insight Genomics, Cat #: RP027) and rabbit anti-goat IgG (BioRad Labs, Cat. #: 172-1034) target Abs were dispensed on the PC microcavities within the OCSS. On arm 4, the PC microcavity A is printed with rabbit anti-goat IgG Abs. After overnight incubation and washing, the device was coated with bovine serum albumin (BSA) to prevent any non-specific binding and washed. The PC microcavity in arm 3 and the second PC microcavity B in arm 4 were thus effectively covered with BSA and served as control microcavities for biomolecule binding. The device was kept wet in PBS at all times.

4 Device characterization

Light is guided in and out of the PCW by ridge waveguides from the MMI with PC group index taper to enable high coupling efficiency into the slow light guided mode.[12] Devices were tested with TE-polarized light by end-fire coupling method with polarization maintaining single-mode tapered-lensed fibers. All probe Abs are introduced in PBS which forms the top cladding. When probe Abs that are specific to their conjugate target Abs on the different arms are introduced, the conjugate specific binding causes a change in the refractive index in the immediate vicinity of the corresponding PC microcavity leading to a change in resonance frequency and hence a shift in wavelength of the dropped resonance from the transmission spectrum of the PCW in the corresponding arm of the MMI. The magnitude of the shift gives a precise interpretation of the concentration of probe Abs.

4.1 Single PC microcavity biosensor characterization

The resonance spectrum of the L13 PC microcavity was first measured in PBS, functionalized with target receptor Abs. The transmission spectrum of the OCSS with the coupled L13 PC microcavity is shown in Fig. 4(a). The resonance wavelength is at 1578.9 nm, near the band edge at 1588 nm, with approximately 12 dB extinction ratio. The corresponding mode profile of the microcavity coupled resonance mode was shown in Fig. 3(b).

The resonance wavelength shift *versus* concentration of probe Abs on arms #1 and #2 were first separately characterized for different concentrations of rat anti-human IL-10 (Invitrogen, Cat #: RHC1K1001) (molecular weight MW = 150 kDa) and goat anti-rabbit IgG (Cat. #: 170-6515) probe Abs (MW = 150 kDa) and the results shown in Fig. 4(b).

Before a new addition of antibody solution carrying a different type of probe protein, the resonance wavelength was measured (λ_1).

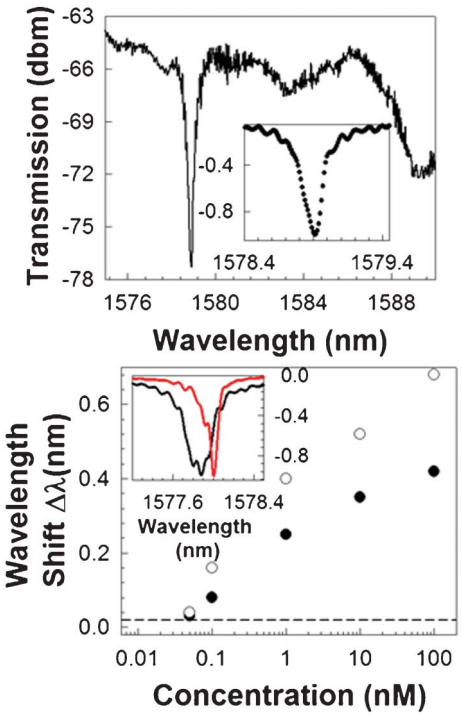

Fig. 4 (a) Transmission spectrum of W1 PCW with coupled L13 PC microcavity. (Inset) shows the normalized transmission, magnifying the wavelength range around the resonance. (b) Wavelength shift of the resonance shown by arrow in (a) as a function of concentration of probe antibodies, rat anti-Human IL-10 (open circles) and goat anti-rabbit IgG (filled circles). (inset) shows the spectral shift from black to red curve when 0.1 nM of probe rat anti-Human IL-10 antibodies is added to a 0 nM PBS background. Dashed line indicates detection limit.

For each concentration of newly added probe antibody solution, the chip was incubated in the probe antibody solution and the resonance wavelength monitored as a function of time. No resonance wavelength shift was observed for 20 min. After 20 min, the resonance wavelength increased as a function of time, until the shift saturated after another 20 min at λ_2. The chip was next washed 3 times in PBS to remove unbound probe Abs and the resonance wavelength λ_3 ($< \lambda_2$) measured again. The final resonance wavelength shift, $\Delta\lambda$, as plotted in Fig. 4(b) is given by $\Delta\lambda = \lambda_3 - \lambda_1$.

A larger wavelength shift is observed in Fig. 4(b) with the probe Ab solution of rat anti-human IL-10 Abs than goat anti-rabbit IgG Abs. The difference in wavelength shifts for the two Abs is related to the lower dissociation constant K_d of rat anti-human IL-10 Abs ($K_d \sim 10^{-10}$ M) than goat anti-rabbit IgG ($K_d \sim 10^{-6}$ M), the details of which are being submitted in a concurrent paper.

A typical resonance shift upon specific binding for the high-Q L13 PC microcavity resonance of 0.1 nM rat anti-human Abs to Human IL-10 Abs is shown in the inset of Fig. 4(b).

The experimentally confirmed Q-factor is approximately 9300. Our previous W1 coupled L7 PC microcavity device,[7] with seven missing holes, in SOI structures had a Q-factor approximately 7300. $Q \approx 9300$ represents the highest Q reported for biosensing in SOI PC devices. 60 μl of probe Abs was directly dispensed from a micro-pipette. Note that only the probe Abs are dispensed with the micro-pipette, as in a diagnostic scenario where the sample will be directly dispensed on the microarray

chip. The target receptor Abs was ink-jet printed. Based on dispensed spot diameter of approx. 8 mm, the L13 PC microcavities can thus detect the binding of 7.5 ng ml^{-1} of rat anti-human IL-10 probe Abs. From Fig. 3(b) inset, considering a sensing area of approx. 11 μm^2 (integrating over a surface where the E-field intensity is more than 50% of maximum value and including the inner surface area of peripheral holes),[7] and uniform surface coverage, the estimated detection limit, without considering unbound Abs that are washed away in L13 devices is 98 atto-grams for rat anti-human IL-10 probe Abs. In Ref. 13, at a concentration of 0.67 nM of probe biomolecules with $K_d \approx 6 \times 10^{-7}$ M, the authors observed a resonance wavelength shift less than 0.05 nm with resonances that had $Q \approx 300$. In contrast, the interpolated resonance wavelength shift that would be observed in our L13 PC microcavity device (from Fig. 4) for biomolecules with $K_d \approx 10^{-6}$ M is about 0.2 nm. The diffusion limited time limit for sensing can be reduced in the future by choosing a smaller volume of dispensed probe solution and/or by incorporating a flow cell into our measurements.

4.2 MMI coupled PC biosensor characterization

The multiplexing experiment is performed with the device in Fig. 1. Results from each arm of the MMI are shown in Fig. 5(a)–(c). 60 µl of 600 nM of goat anti-rabbit IgG Abs in PBS is introduced which causes a resonance wavelength shift in arm 2 that is printed with its specific conjugate rabbit anti-goat IgG Abs. A similar shift is observed in the PC microcavity A in arm 4 of the MMI. No shift is observed in arm 1, printed with human IL-10 Abs, which is not specific to the introduced probe Abs. Similarly, no shift is observed in arm 3 or in the PC microcavity B in arm 4 that was coated with BSA. Next, 60 µl of 600 nM of rat anti-human IL-10 Abs in PBS is introduced. A resonance wavelength shift is observed in arm 1 of the MMI that was printed with its specific target conjugate Human IL-10 Abs. No resonance wavelength shift is observed in the other arms. Fig. 5(d) shows the transmission spectrum of the W1 PCW in arm 4 of the MMI with the two coupled L13 microcavities with slightly different geometry as described earlier. The resonances corresponding to PC microcavities A and B are at 1565 nm and 1573 nm respectively. Fig. 5(d) shows the resonance wavelength shift observed in the W1 PCW in arm 4 in A at 1565 nm when 1 nM of probe goat anti-rabbit IgG Abs in PBS is added. No shift is observed in B at 1573 nm.

Our current measurement setup can only measure one waveguide at a time; however, one can couple outputs from all waveguides to a multi-core optical fiber to enable all measurements to be monitored simultaneously for high throughput biosensing.

5 Conclusions

In summary, we demonstrated an on-chip sensing subsystem for high-throughput, high-sensitivity biosensing with MMI power splitters and multiple PC microcavities coupled to PCWs. In addition to the highest Q observed in bio-ambient PBS with SOI-based PC microcavity devices, which enables higher accuracy, we observed more than an order of magnitude higher Q and four times-larger resonance wavelength shift than previous demonstrations.[13] The present demonstration interrogates five PC microcavities simultaneously, that recognize different specific binding

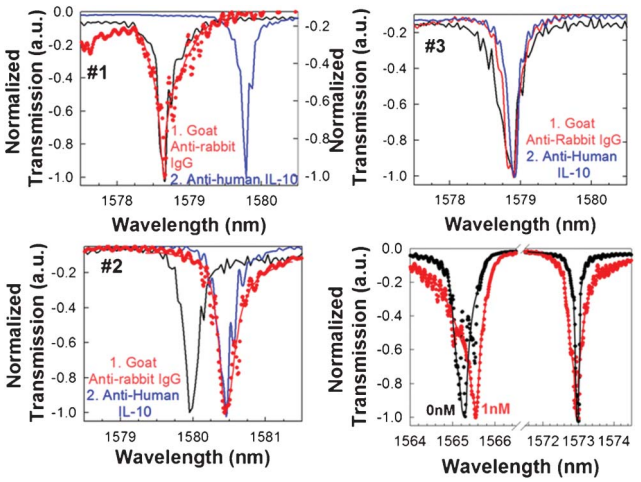

Fig. 5 Resonance wavelength shift or none thereof observed in the (a)–(c) L13 PC microcavities in arms 1–3 of the 1 × 4MMI when probe antibodies goat anti-rabbit IgG in PBS and rat anti-human IL-10 in PBS are added in sequence and (d) arm 4 of the 1 × 4MMI with 1 nM of probe antibodies of goat anti-rabbit IgG in PBS.

interaction between target and probe antibody conjugates. Based on past designs,[9] future devices will extend to larger arrays for simultaneous high throughput high sensitivity measurement that will benefit the microarray end-user community in diverse fields.

Acknowledgements

The authors acknowledge the National Cancer Institute for supporting this work under the Small Business Innovation Research (SBIR) program (Contract # HHSN261201000085C).

References

1 M. F. Templin, D. Stoll, J. M. Schwenk, O. Potz, S. Kramer and T. O. Joos, *Proteomics*, 2003, **3**, 2155.
2 M. Iqbal, M. A. Gleeson, B. Spaugh, F. Tybor, W. G. Gunn, M. Hochberg, T. Baehr-Jones, R. C. Bailey and L. C. Gunn, *IEEE J. Sel. Top. Quantum Electron.*, 2010, **16**, 654.
3 C. F. Carlborg, K. B. Gylfason, A. Kazmierczak, F. Dortu, M. J. Banuls Polo, A. Maquieira Catala, G. M. Kresbach, H. Sohlstrom, T. Moh, L. Vivien, J. Popplewell, G. Ronan, C. A. Barrios, G. Stemme and W. van der Winjgaart, *Lab Chip*, 2010, **10**, 281.
4 A. Densmore, M. Vachon, D. X. Xu, S. Janz, R. Ma, Y. H. Li, G. Lopinski, A. Delage, J. Lapointe, C. C. Luebbert, Q. Y. Liu, P. Cheben and J. H. Schmid, *Opt. Lett.*, 2009, **34**, 3598.
5 H. Sipova, S. Zhang, A. M. Dudley, D. Galas, K. Wang and J. Homola, *Anal. Chem.*, 2010, **82**, 10110.
6 S. Chakravarty, J. Topoľančik, P. Bhattacharya, S. Chakrabarti, Y. Kang and M. E. Meyerhoff, *Opt. Lett.*, 2005, **30**, 2578.
7 W-C. Lai, S. Chakravarty, Y. Zou, C-Y. Lin and R. T. Chen, *Opt. Lett.*, 2012, **37**, 1208.
8 S. Pal, E. Guillermain, R. Sriram, B. L. Miller and P. M. Fauchet, *Biosens. Bioelectron.*, 2011, **26**, 4024.
9 A. Hosseini, D. N. Kwong, H. Subbaraman, Y. Zhang, X. Xu and R. T. Chen, *IEEE J. Sel. Top. Quantum Electron.*, 2011, **17**, 510.
10 Y. Akahane, T. Asano, B-S. Song and S. Noda, *Nature*, 2003, **425**, 944.
11 A. Subramanian, S. J. Kennel, P. I. Oden, K. B. Jacobson, J. Woodward and M. J. Doktycz, *Enzyme Microb. Technol.*, 1999, **24**, 26.
12 C-Y. Lin, X. Wang, S. Chakravarty, B-S. Lee, W-C. Lai and R. T. Chen, *Appl. Phys. Lett.*, 2010, **97**, 183302.
13 S. Zlatanovic, L. W. Mirkarimi, M. M. Sigalas, M. A. Bynum, E. Chow, K. M. Robotti, G. W. Burr, S. Esener and A. Grot, *Sens. Actuators, B*, 2009, **13**, 141.